Co-registered photoacoustic and fluorescent imaging of a switchable nanoprobe based on J-aggregates of indocyanine green

Diego S. Dumani, Hans-Peter Brecht, Vassili Ivanov, Ryan Deschner, Justin T. Harris, et al.

Diego S. Dumani, Hans-Peter Brecht, Vassili Ivanov, Ryan Deschner, Justin T. Harris, Kimberly A. Homan, Jason R. Cook, Stanislav Y. Emelianov, Sergey A. Ermilov, "Co-registered photoacoustic and fluorescent imaging of a switchable nanoprobe based on J-aggregates of indocyanine green," Proc. SPIE 10494, Photons Plus Ultrasound: Imaging and Sensing 2018, 104942W (28 February 2018); doi: 10.1117/12.2291262

SPIE.

Event: SPIE BiOS, 2018, San Francisco, California, United States

Co-registered photoacoustic and fluorescent imaging of a switchable nanoprobe based on J-aggregates of indocyanine green

Diego S. Dumani[a,b], Hans-Peter Brecht[c], Vassili Ivanov[c], Ryan Deschner[d], Justin T. Harris[d], Kimberly A. Homan[d], Jason R. Cook[d], Stanislav Y. Emelianov[a,b*], Sergey A. Ermilov[c**]

[a]Wallace H. Coulter Department of Biomedical Engineering, Georgia Institute of Technology and Emory University School of Medicine, Atlanta, GA 30332
[b]School of Electrical and Computer Engineering, Georgia Institute of Technology, Atlanta, GA 30332
[c]PhotoSound Technologies, Inc., Houston, TX 77081
[d]NanoHybrids, Inc., Austin, TX 78744

ABSTRACT

We introduce a preclinical imaging platform – a 3D photoacoustic/fluorescence tomography (PAFT) instrument augmented with an environmentally responsive dual-contrast biocompatible nanoprobe. The PAFT instrument was designed for simultaneous acquisition of photoacoustic and fluorescence orthogonal projections at each rotational position of a biological object, enabling direct co-registration of the two imaging modalities. The nanoprobe was based on liposomes loaded with J-aggregates of indocyanine green (PAtrace). Once PAtrace interacts with the environment, a transition from J-aggregate to monomeric ICG is induced. The subsequent recovery of monomeric ICG is characterized by dramatic changes in the optical absorption spectrum and reinstated fluorescence. In the activated state, PAtrace can be simultaneously detected by both imaging modes of the PAFT instrument using 780 nm excitation and fluorescence detection at 810 nm. The fluorescence imaging component is used to boost detection sensitivity by providing low-resolution map of activated nanoprobes, which are then more precisely mapped in 3D by the photoacoustic imaging component. Activated vs non-activated particles can be distinguished based on their different optical absorption peaks, removing the requirements for complex image registration between reference and detection scans. Preliminary phantom and *in vivo* animal imaging results showed successful activation and visualization of PAtrace with high sensitivity and resolution. The proposed PAFT-PAtrace imaging platform could be used in various functional and molecular imaging applications including multi-point *in vivo* assessment of early metastasis.

Keywords: Photoacoustic tomography, photoacoustic imaging, fluorescence, multimodal imaging, preclinical imaging, lymph node, contrast agent, molecular imaging

1. INTRODUCTION

Numerous biomarkers play a significant role in medical imaging for oncology, cardiology, immunology, among other areas. Identifying the presence of different types of molecules and cells, together with environmental cues, such as pH and oxygenation, can be critical for diagnosis, therapy and monitoring of disease.

Contrast agents are commonly used to enable and enhance biomarker visualization[1-7]. In many cases, imaging applications can further benefit from responsive contrast agents that are able to interact and change with the environment, elucidating the status of one or more biomarkers. Examples include imaging of cancer cells[8, 9], immune cells[10, 11], pH[12, 13] or enzyme activity[14, 15].

The choice of imaging modality is dependent on the desired sensitivity, spatial and temporal resolution, cost, safety, and the ability to provide structural, functional or molecular information. Unfortunately, no single modality excels in all these attributes[16, 17]. Particularly, technologies such as PET and fluorescence imaging exhibit high sensitivity but suffer from poor spatial resolution. Conversely, others such as MRI, ultrasound, and photoacoustic imaging allow superior resolution at the expense of limited sensitivity due to lower signal-to-background ratio. By using multimodal imaging approaches, high resolution images may be achieved while synergistically boosting detection sensitivity[18, 19].

*stas@gatech.edu; **sae@pst-inc.com

Photons Plus Ultrasound: Imaging and Sensing 2018, edited by Alexander A. Oraevsky, Lihong V. Wang, Proc. of SPIE Vol. 10494, 104942W · © 2018 SPIE · CCC code: 1605-7422/18/$18 · doi: 10.1117/12.2291262

Previously, we introduced the use of liposome-encapsulated J-aggregates of indocyanine green (ICG) (Fig. 1A), named *PAtrace*, as an environment responsive agent for photoacoustic imaging (PA)[20, 21]. This contrast agent has an optical absorption peak at 890 nm that blue-shifts to 780 nm upon interaction with cells or environment (Fig. 1B). This shift is caused by the rupture of the liposome, which releases the ICG J-aggregate, subsequently breaking down into free ICG molecules. Besides the absorption spectrum shift, detectable via photoacoustic imaging, the process also enables fluorescence emission detected above 800 nm, a long-known characteristic of ICG[22-24].

In this paper we took advantage of the multimodality of PAtrace, by using a platform integrating a 3D photoacoustic/fluorescence tomography (PAFT) instrument. The system simultaneously acquires both imaging components using the same laser pulse as excitation, thus allowing co-registration. First, we show phantom results validating the photoacoustic detection prior to activation, and multimodal detection after activation. Last, we show *in vivo* results of particle drainage and activation in a murine inguinal lymph node.

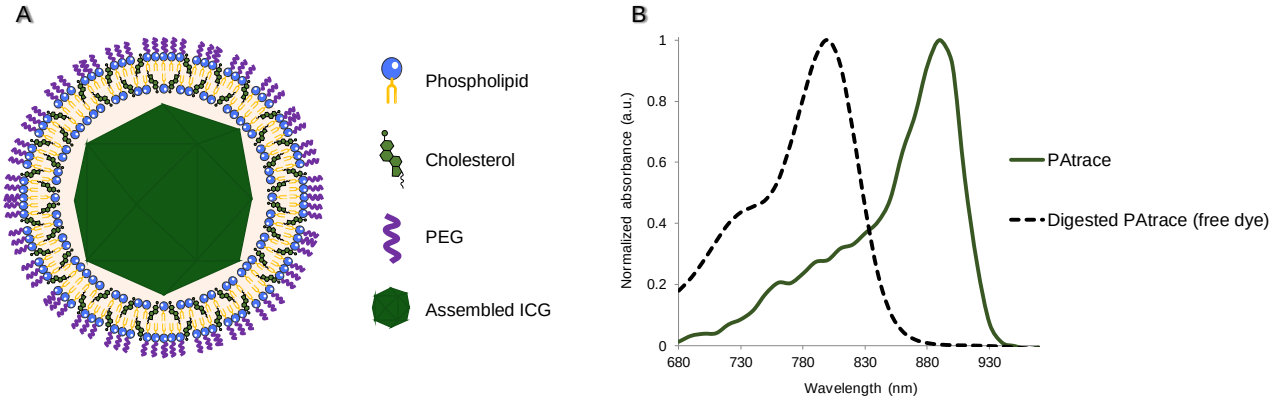

Figure 1. (A) Schematic of PAtrace shows an ICG J-aggregate encapsulated by a phospholipid and cholesterol shell. (B) Absorption spectra of intact and digested PAtrace. Before interaction, a sharp peak at 890 nm is obtained. After interaction with cells or environment, free ICG absorption spectrum is recovered.

2. MATERIALS AND METHODS

2.1 Photoacoustic/Fluorescence imaging setup

Tomographic photoacoustic and fluorescence imaging was simultaneously performed using a PAFT system, as described by Brecht *et al* [25]. Briefly, the sample holder is vertically inserted in a water tank where laser excitation is delivered by four orthogonal fiberoptic illuminators, using a Phocus Mobile tunable laser (Opotek Inc). The laser can be tuned between 690 nm and 970 nm, with a 10 Hz repetition rate, and 5 ns pulse duration. Fluence at the phantom or skin surface was kept below the American National Standard Institute (ANSI) safety limits. Photoacoustic images are acquired with a 96-element array transducer, 6 MHz center frequency. Fluorescence is acquired with a scientific CMOS camera Dhyana 400D (Tucsen Photonics) equipped with a fluorescence emission filter matching the emission spectrum of ICG. During the scan, the sample rotates at $10°\cdot s^{-1}$ while tomographic slices are registered for full-volume offline reconstruction using standard filtered backprojection.

2.2 Phantom imaging

A phantom was designed containing five ultrathin wall polytetrafluoroethylene (PTFE) tubes, 0.9 mm diameter (Zeus, Inc.). Each tube was filled with a different contrast agent as represented in Fig. 2A. Optical densities of the agents were matched to OD = 5 cm^{-1} at their respective absorption peak. The phantom included PAtrace in DI water, PAtrace in Triton X-100, free ICG solution, and cupric sulfate ($CuSO_4$) solution. Triton X-100 is a surfactant that breaks down liposomes and monomerizes the ICG, simulating the activation and environment interaction that particles would undergo *in vivo*. The $CuSO_4$ solution was used as a reference to normalize wavelength-dependent laser fluence variations.

The tube ends were sealed with glue to prevent leakage, and one hour was allowed for the glue to dry. Then, the phantom was placed vertically in the sample holder and inserted into the water tank (temperature = 25 °C). Images were acquired using 780 nm (multimodal) and 890 nm (PA only) laser excitation.

2.3 *In vivo* imaging

A naïve mouse (Nu/Nu, Charles River Laboratories) was used as part of a protocol approved by the Institutional Animal Care and Use Committee (IACUC) at the Georgia Institute of Technology. The animal was injected with 40 µl of PEGylated PAtrace (OD = 80 cm^{-1}) in the right caudal mammary fat pad. The particles were allowed to drain to the inguinal lymph node for 24 hours. The mouse was then anesthetized and positioned in a restrainer with a free-breathing anesthesia delivery system (Fig. 3). The restrainer was vertically placed in the sample holder and inserted into the water tank. Water temperature was kept at 37 °C. Images were then acquired using 780 nm (multimodal) and 890 nm (PA only) wavelengths.

3. RESULTS AND DISCUSSION

The results of the PAFT phantom imaging showed successful detection of PAtrace activation, both photoacoustically and fluorescently. Upon activation, PAtrace is expected to lose 890-nm absorption, and gain 780-nm absorption, together with reinstated fluorescence. The free ICG solution displayed a similar behavior to that of digested PAtrace, as expected.

A front view of the phantom (Fig. 2B) shows no fluorescence for intact PAtrace, and high fluorescence emission for digested PAtrace, as well as free ICG. While all tubes are in the field of view, only tubes 2 and 3 are visible. Tube 1, and support rods are slightly discernible, due to a small leakage of excitation light. At 890 nm, only intact PAtrace was detected via PA imaging (Fig. 2C). PA images at 780 nm show high contrast for activated PAtrace and free ICG, but low signal when PAtrace is intact (Fig. 2D).

The tube containing $CuSO_4$ showed no fluorescence. It was photoacoustically detected both at 890 nm and 780 nm. Due to its known absorption spectrum, it was used to normalize PA intensities and account for wavelength-dependent laser fluence variations. The tube with DI water was not visible with either modality, showing that the PTFE tubes had no contribution to background signal.

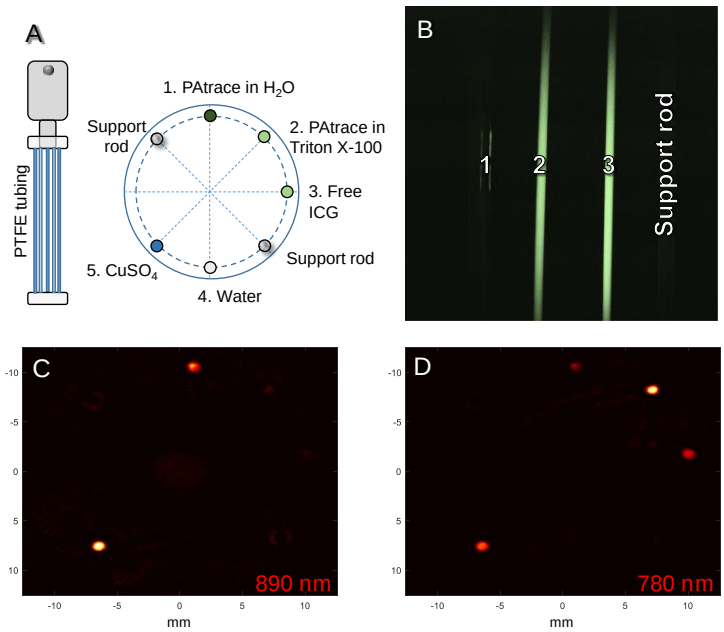

Figure 2. (A) Schematic of PAFT phantom design. On the left is the phantom, on the right is a horizontal slice view. (B) Fluorescence image showing tubes 1, 2, and 3, using 780 nm excitation. Tubes 4, 5, and support rods are not visible. (C) Horizontal slice view of PA at 890 nm. (D) Horizontal slice view of PA at 780 nm. The tubes' positions are matched in (A), (C), and (D) horizontal slices.

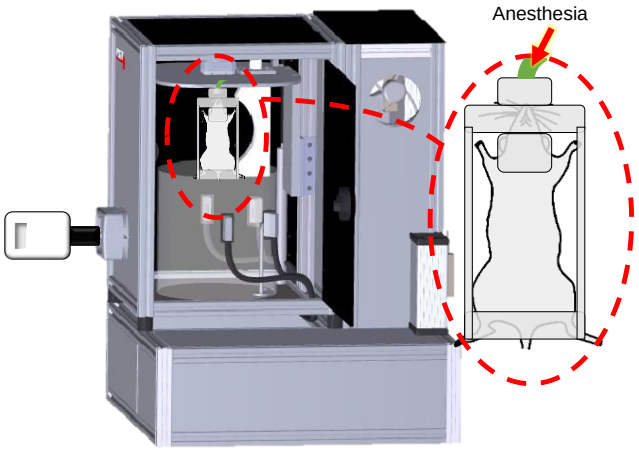

Figure 3. Schematic of mouse restrainer and its position in PAFT system.

In vivo results showed feasibility of this platform for use in preclinical studies. The injection site and draining lymph node were clearly identified in PA images at 780 nm (Fig. 4). Endogenous absorption, coming predominantly from deoxygenated blood, was also visible. On the other hand, fluorescent images showed high emission at the lymph node but very low background signals. High PA contrast and fluorescence at 780 nm excitation indicate activation of PAtrace, most likely due to cellular uptake. This suggests that the contrast agent may have been endocytosed at the injection site and then trafficked to the lymph node via immune cells. Another possibility is that the particles were also digested by resident cells after passive drainage to the lymph node occurred.

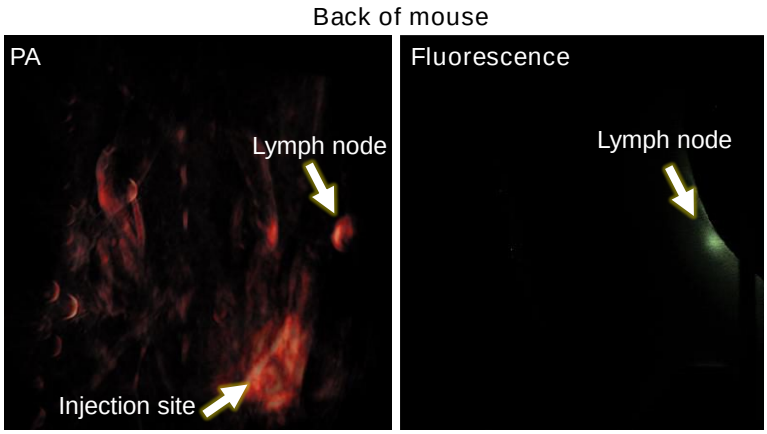

Figure 4. Photoacoustic (PA) 2D projection and fluorescence images of a mouse (dorsal view) using 780 nm laser excitation.

By using a responsive multimodal agent, there is no requirement for complex image registration between reference and detection scans. Thus, imaging before injection is not needed. In this study, the PEGylated PAtrace particles were not targeted to any specific type of cell. Because of this, we injected a solution with a high optical density to maximize non-specific cellular uptake and particle activation. In the future, the phospholipid shell of PAtrace could be functionalized in order to interact with specific cell types, molecules, or environmental cues. Then, a much lower amount of contrast agent would be needed, given the potentially higher uptake activity, together with the sensitivity boost that fluorescence provides. Additionally, PA imaging of endogenous absorbers could also be used to complement the obtained molecular information with functional parameters such as blood oxygenation.

4. CONCLUSIONS

We presented a combined photoacoustic/fluorescence tomography (PAFT) imaging system augmented with an environment responsive contrast agent (PAtrace). The synergy of photoacoustic and fluorescent imaging modalities can be exploited to enhance sensitivity and resolution of PAFT system. We showed successful activation and detection of PAtrace in a phantom and *in vivo*. The introduced approach can be used in various applications including oncology, cardiology, immunology, and many others. Future studies will include surface functionalization of the contrast agent for applications ranging from lymph node metastasis detection to atherosclerotic plaque characterization.

ACKNOWLEDGEMENTS

This work was partially supported by National Institutes of Health under grants R43OD023029 and R43CA224824, and Breast Cancer Research Foundation grant BCRF-16-043.

REFERENCES

[1] Santiesteban, D. Y., Kubelick, K., Dhada, K. S., Dumani, D., Suggs, L., and Emelianov, S., "Monitoring/Imaging and Regenerative Agents for Enhancing Tissue Engineering Characterization and Therapies," Annals of biomedical engineering, 44(3), 750-772 (2016).

[2] Luke, G. P., Yeager, D., and Emelianov, S. Y., "Biomedical applications of photoacoustic imaging with exogenous contrast agents," Annals of biomedical engineering, 40(2), 422-437 (2012).

[3] Cook, J. R., Dumani, D. S., Kubelick, K. P., Luci, J., and Emelianov, S. Y., "Prussian blue nanocubes: multi-functional nanoparticles for multimodal imaging and image-guided therapy (Conference Presentation)," SPIE Photons Plus Ultrasound: Imaging and Sensing. 10064, 100641T (2017).

[4] Pierce, M. C., Javier, D. J., and Richards-Kortum, R., "Optical contrast agents and imaging systems for detection and diagnosis of cancer," International journal of cancer, 123(9), 1979-1990 (2008).

[5] Ntziachristos, V., Bremer, C., and Weissleder, R., "Fluorescence imaging with near-infrared light: new technological advances that enable in vivo molecular imaging," European radiology, 13(1), 195-208 (2003).

[6] Bremer, C., Ntziachristos, V., and Weissleder, R., "Optical-based molecular imaging: contrast agents and potential medical applications," European radiology, 13(2), 231-243 (2003).

[7] Bulte, J. W., and Kraitchman, D. L., "Iron oxide MR contrast agents for molecular and cellular imaging," NMR in Biomedicine, 17(7), 484-499 (2004).

[8] Luke, G. P., Myers, J. N., Emelianov, S. Y., and Sokolov, K. V., "Sentinel lymph node biopsy revisited: ultrasound-guided photoacoustic detection of micrometastases using molecularly targeted plasmonic nanosensors," Cancer Research, 74(19), 5397-5408 (2014).

[9] Durr, N. J., Larson, T., Smith, D. K., Korgel, B. A., Sokolov, K., and Ben-Yakar, A., "Two-photon luminescence imaging of cancer cells using molecularly targeted gold nanorods," Nano letters, 7(4), 941-945 (2007).

[10] Dumani, D., Sun, I.-C., and Emelianov, S., "In vivo photoacoustic detection of lymph node metastasis using glycol-chitosan-coated gold nanoparticles," IEEE International Ultrasonics Symposium (IUS). 1-4 (2017).

[11] Weissleder, R., Nahrendorf, M., and Pittet, M. J., "Imaging macrophages with nanoparticles," Nature materials, 13(2), 125 (2014).

[12] Wang, C., Cheng, L., Liu, Y., Wang, X. *et al.*, "Imaging-Guided pH-Sensitive Photodynamic Therapy Using Charge Reversible Upconversion Nanoparticles under Near-Infrared Light," Advanced Functional Materials, 23(24), 3077-3086 (2013).

[13] Chen, Y., Yin, Q., Ji, X., Zhang, S. *et al.*, "Manganese oxide-based multifunctionalized mesoporous silica nanoparticles for pH-responsive MRI, ultrasonography and circumvention of MDR in cancer cells," Biomaterials, 33(29), 7126-7137 (2012).

[14] Razansky, D., Harlaar, N. J., Hillebrands, J. L., Taruttis, A. *et al.*, "Multispectral optoacoustic tomography of matrix metalloproteinase activity in vulnerable human carotid plaques," Molecular imaging and biology, 14(3), 277-285 (2012).

[15] de Vries, B. M. W., Hillebrands, J.-L., van Dam, G. M., Tio, R. A. *et al.*, “Multispectral Near-Infrared Fluorescence Molecular Imaging of Matrix Metalloproteinases in a Human Carotid Plaque Using a Matrix-Degrading Metalloproteinase–Sensitive Activatable Fluorescent Probe,” Circulation, 119(20), e534-e536 (2009).
[16] Frangioni, J. V., “New technologies for human cancer imaging,” Journal of clinical oncology, 26(24), 4012-4021 (2008).
[17] Weissleder, R., and Pittet, M. J., “Imaging in the era of molecular oncology,” Nature, 452(7187), 580 (2008).
[18] Lovell, J. F., Jin, C. S., Huynh, E., Jin, H. *et al.*, “Porphysome nanovesicles generated by porphyrin bilayers for use as multimodal biophotonic contrast agents,” Nature materials, 10(4), 324 (2011).
[19] Sun, I.-C., Dumani, D. S., and Emelianov, S. Y., "Multimodal imaging of lymph nodes and tumors using glycol-chitosan-coated gold nanoparticles (Conference Presentation)," SPIE Photons Plus Ultrasound: Imaging and Sensing. 10064, 100640Y (2017).
[20] Harris, J. T., Dumani, D. S., Cook, J. R., Sokolov, K. V., Emelianov, S. Y., and Homan, K. A., "Assessment of plaque vulnerability in atherosclerosis via intravascular photoacoustic imaging of targeted liposomal ICG J-aggregates (Conference Presentation)," SPIE Photons Plus Ultrasound: Imaging and Sensing 10064, 1006413 (2017).
[21] Harris, J. T., Dumani, D. S., Cook, J. R., Sokolov, K. V., Emelianov, S. Y., and Homan, K. A., "Identification of M1 Macrophages in Vulnerable Plaques With Folate Receptor Beta Targeted Liposomal Indocyanine Green J-Aggregates," Circulation. 134, A19605 (2016).
[22] Landsman, M., Kwant, G., Mook, G., and Zijlstra, W., “Light-absorbing properties, stability, and spectral stabilization of indocyanine green,” Journal of applied physiology, 40(4), 575-583 (1976).
[23] Hayashi, K., Hasegawa, Y., and Tokoro, T., “Indocyanine green angiography of central serous chorioretinopathy,” International ophthalmology, 9(1), 37-41 (1986).
[24] Benson, R., and Kues, H., “Fluorescence properties of indocyanine green as related to angiography,” Physics in Medicine & Biology, 23(1), 159 (1978).
[25] Brecht, H. P., Ivanov, V., Dumani, D. S., Emelianov, S. Y., Anastasio, M. A., and Ermilov, S. A., "A 3D imaging system integrating photoacoustic and fluorescence orthogonal projections for anatomical, functional and molecular assessment of rodent models," SPIE Photons Plus Ultrasound: Imaging and Sensing. 10494(2018).